Journal of the European Ceramic Society 44 (2024) 5308–5318

Contents lists available at ScienceDirect

Journal of the European Ceramic Society

journal homepage: www.elsevier.com/locate/jeurceramsoc

Thermo-oxidative resistance of C-rich SiCN(O) nonwovens influenced by the pretreatment of the silazane

Heloisa Ramlow [a], Luiz Fernando Belchior Ribeiro [b], Stefan Schafföner [c], Günter Motz [c,*], Ricardo Antonio Francisco Machado [a]

[a] Graduate Program in Chemical Engineering, Federal University of Santa Catarina, Universitário Reitor João David Ferreira Lima Campus, 88040-900 Florianópolis, Brazil
[b] Department of Energy and Sustainability, Federal University of Santa Catarina, Pedro João Pereira 150, 88905-120 Araranguá, Brazil
[c] Chair of Ceramic Materials Engineering, University of Bayreuth, Prof. Rüdiger Bormann-Str. 1, 95447 Bayreuth, Germany

ARTICLE INFO

Keywords:
Electrospinning
Polymer-derived ceramics
Preceramic polymers
Polyacrylonitrile
Oxidation resistance

ABSTRACT

C-rich SiCN(O) ceramic nonwovens with thermo-oxidation resistance up to 600 °C were developed from electrospinning of polyacrylonitrile in combination with different ratios of an oligomeric or polymeric silazane and subsequent pyrolysis. The influence of the selective pre-polymerization of the oligosilazane and the respective amount on the electrospinning, pyrolysis, phase formation and the properties of the resulting C-rich ceramic nonwovens was evaluated. The fiber diameter after pyrolysis at 1000 °C ranges from 0.26 to 0.63 μm. The oligosilazane/PAN-derived ceramic nonwovens contain high oxygen and carbon content because of high reactivity leading to a high ceramic yield due to additional crosslinking. A higher initial oxidation temperature compared to pure carbon was confirmed for all samples. However, the best result was achieved with a sample based on a high proportion of polysilazane in combination with PAN, as a dense passivating layer to protect the free carbon regions was obviously better able to form.

1. Introduction

Since the development of the first electrochemical devices, carbon materials have been extensively used as catalysts and/or catalytic supports for applications such as batteries, supercapacitors, fuel cells, electrochemical sensors, and several electrolysis processes [1–3]. Among the various advantages that justify the relevance of carbon in such applications, are its high conductivity, good thermal and chemical stability, processing versatility, and low cost [4]. However, its susceptibility to oxidation at high temperatures or in the presence of strong oxidizing agents potentially reduces its performance or even limits its applications [5,6].

To enhance catalytic performance, the development of the catalytic supports must present a high surface area to provide more active sites for reactions to take place. One interesting strategy that has been explored in recent years, is the processing of carbon nanofibers by using electrospinning [7–9]. Nonetheless, while increasing surface area leads to improved catalytic activity, the challenges of avoiding thermo-oxidative issues also increase.

Si-based ceramics processed by the polymer-derived ceramics (PDCs) route often fulfill the growing demand for lightweight and thermo-oxidative resistant materials. PDCs present excellent resistance in harsh environments and, as they are obtained through the pyrolysis of a polymeric precursor, they allow the manufacturing of ceramics in complex shapes [10–16]. However, despite their good chemical and thermal stability, PDCs have low electrical conductivity, which is essential in, for example, electrolysis and other electron transfer processes. For this reason, different alternatives are investigated by combining the PDC technology with carbon precursors. The so-called C-rich PDCs represent an excellent alternative benefitting from the properties of the two phases [17] and are been explored in several interesting electrochemical applications, such as anodes in lithium-ion batteries [18–21] or very robust catalytic supports [22,23].

Reports on electrospinning of carbon-rich PDCs are still scarce in the literature, although both technologies are well established. For instance, SiCN and SiCBN doped carbon nanofibers were prepared through the PDC route via electrospinning [24]. Although the authors have reported an improvement in oxidation resistance, the results are still limited to

* Corresponding author.
E-mail address: guenter.motz@uni-bayreuth.de (G. Motz).

https://doi.org/10.1016/j.jeurceramsoc.2024.01.035
Received 13 September 2023; Received in revised form 3 January 2024; Accepted 10 January 2024
Available online 14 January 2024

Table 1
Solutions' characteristics and operating conditions of electrospinning of samples containing oligosilazane or polysilazane.

Name	Solutions' characteristics			Operating conditions of electrospinning		
	Total polymer concentration in DMF (wt %)	D1800/PAN ratio (wt %)	HTTS/PAN ratio (wt %)	Voltage (kV)	Feed rate ($ml \cdot h^{-1}$)	Tip-to-collector-distance (cm)
D1800_PAN	17.5	3:2	-	21	0.8	23.5
HTTS_PAN	17.5	-	3:2	21	0.8	23.5
PAN_D1800	15.0	3:7	-	21	0.2	23.5
PAN_HTTS	13.0	-	3:7	21	0.2	23.5

the carbon phase properties, since it was not possible to notice a shift in the beginning of oxidation to higher temperature accompanied by a large mass loss during oxidation tests. This limited improvement can be attributed to the low concentration of ceramic precursor used in the system, which is probably insufficient to provide the desired oxidation protection. More recently, Liao et al. reported the obtaining of C/SiCON electrospun nonwoven materials with very interesting multifunctional properties, combining extremely low thermal conductivity and high electrical conductivity [25]. Also, due to the well-distributed carbon/-ceramic phase, the material showed remarkable fire resistance, comparable to commercial ceramic materials even presenting almost 50 wt% of carbon.

In this study, the influence of an oligomeric or polymeric silazane, each in combination with PAN, on the electrospinning process and thermo-oxidative properties of the resulting carbon-rich ceramic nonwovens were investigated. Especially, the effect of performing a selective pre-crosslinking on the used silazane was evaluated, since the increase in its molecular weight impacts both its processing behavior by electrospinning, its ceramic yield after pyrolysis and the resulting properties. It is hypothesized that besides the variation of the silazane/PAN ratio, the degree of polymerization and the cross-linking reactions of the silazane can influence the oxidation stability of the pyrolyzed material which is important for the application as catalyst supports with huge surfaces in harsh environments.

2. Material and methods

2.1. Materials

The commercial silazane Durazane 1800 (Merck KGaA, Germany) was selected as the oligosilazane (hereinafter referred to as D1800) and for the synthesis of the polysilazane named as HTTS by using the catalyst tetra-n butylammonium fluoride 1 M in tetrahydrofuran (THF) (Sigma-Aldrich Co. LLC., Germany) and calcium borohydride bis(tetrahydrofuran) (Sigma-Aldrich Co. LLC., Germany) to terminate the polymerization reaction. Tetrahydrofuran 99.5% and dimethylformamide 99.5% (Fischer Chemical, USA) were employed respectively for synthesis and electrospinning. PAN 200 kDa (Polysciences, USA) was used as the carbon precursor. Dicumyl peroxide (DCP) 98% (Sigma-Aldrich Co. LLC., Germany) was used as the curing initiator.

2.2. Methods

To obtain the solid polysilazane HTTS suitable for electrospinning, the liquid oligosilazane Durazane 1800 was selectively polymerized using a similar procedure reported elsewhere [26]. Briefly, 50 g of Durazane 1800 was dissolved under vigorous magnetic stirring in 140 ml of THF followed by the addition of 0.25 wt% of TBAF as catalyst. After 120 min, an excess of the inhibitor calcium borohydride bis (tetrahydrofuran) was added to stop the reaction. The mixture was stirred for 5 min and then filtered to remove the formed calcium fluoride. THF was removed under reduced pressure. The PAN was dried at 110 °C for 24 h before use. Different solutions were prepared inside a laboratory glass bottle by first stirring PAN in DMF at 100 °C for 3 h. After cooling to room temperature, oligosilazane or polysilazane and 3 wt% DCP in relation to the silazane was added and stirred for 12 h at room temperature. The solutions were electrospun in a nitrogen atmosphere using a lab-scale electrospinning device. The needle diameter corresponded to 21 G (0.8 mm). The concentrations were established based on electrospinnability of each solution defined according to preliminary experiments (Table 1). The samples were denoted as D1800_PAN and PAN_D1800 for oligosilazane, and HTTS_PAN and PAN_HTTS for polysilazane.

The manufactured polymer nonwovens were pyrolyzed in a nitrogen atmosphere from 20 to 1000 °C (5 $K \cdot min^{-1}$), kept at 1000 °C for 1 h, and allowed to cool to room temperature. The resulting C-rich SiCN(O) fiber nonwovens are denoted as D1800_PAN_1000, HTTS_PAN_1000, PAN_D1800_1000, and PAN_HTTS_1000.

The rheological behavior of the solutions was evaluated using a rotational rheometer in parallel plate configuration (MCR 702, Anton Paar, Austria) [27]. The average of two replicates was considered. The surface tension was analyzed through the hanging-drop approach using a drop-shape analyzer (volume per drop of ~4 μL) (DSA25E, Krüss, Germany). The electrical conductivity of the solutions was measured by a conductometer (SevenCompact S230-Basic, Mettler Toledo, EUA). The average of three samples was considered.

Scanning electron microscope (SEM) was used to observe the morphology of the electrospun nonwovens with an acceleration voltage of 3 kV and magnification of × 3000 (Gemini Sigma 300 VP, Zeiss, Germany). The samples were previously sputter-coated with gold (thickness of 280 Å) (Sputter Coater 108auto, Cressington, England) to increase conductivity and improve image visualization. The fiber diameter was evaluated from four different SEM images measuring randomly 100 fibers of each sample with open-source ImageJ software. Fourier transform infrared spectroscopy (FTIR) was conducted using an attenuated total reflection (ATR) sampling unit (Tensor 27, Bruker Corporation, USA). Spectra were min-max normalized for comparison of the samples to overcome the confounding effect of varying sample thickness on the band intensity.

The carbon structure was analyzed through Raman spectroscopy with a 532 nm wavelength laser (Senterra II, Bruker, USA) and X-ray powder diffraction (XRD) using flat-sample transmission geometry with monochromatic Cu K-α radiation (λ = 1.5418 Å, 40 mA, and 40 kV) (D8 Advance, Bruker AXS, Germany). The Raman curves were fitted using the Lorentzian function and Origin 2021b software. The I_D/I_G ratios were calculated based on the area of each band after curve fitting. The crystallite size (L_a) was determined according to the TK-correlation [28].

Solid-state ^{29}Si-nuclear magnetic resonance (NMR) spectra were recorded using 4 mm Bruker probes ($B_0 = 7.05$ T, $\nu_0(^{29}Si) = 59.66$ MHz) and spinning frequency of 10 kHz (Bruker AVANCE II 300, Bruker Corporation, USA). The ^{29}Si-NMR spectra were [0,1] normalized for comparison. X-ray photoelectron spectroscopy (XPS) was conducted using Al $K\alpha^+$ ion beam with an energy of 1486.6 eV and a spot size of 400 μm (Thermo Scientific, Chanhassen, USA). The surface contamination was removed by surface sputtering with argon at 3.0 keV for 2 min

The nonwoven density was determined by helium pycnometry (AccuPyc II 1340, Micromeritics, USA). The surface area was determined via krypton adsorption using BET (ASAP 2010, Micrometrics, USA). Thermal gravimetric analysis (TGA) and differential scanning calorimetry (DSC) were performed by heating from 20 to 1000 °C (5

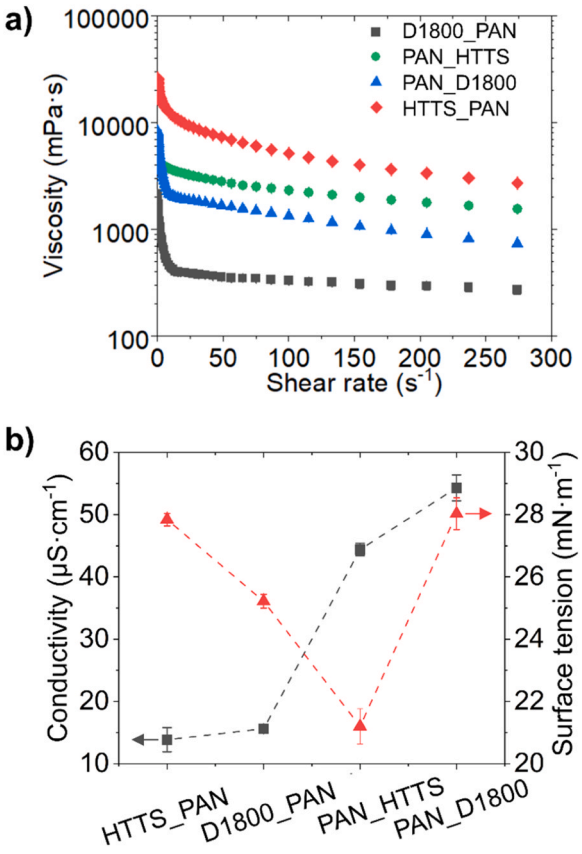

Fig. 1. Properties of the different solutions: a) viscosity as a function of the shear rate and b) conductivity and surface tension.

K·min^{-1}) in a flowing nitrogen atmosphere (~5 mg of the sample) (STA 449 F5 Jupiter, Netzsch GmbH, Germany). For thermo-oxidation tests, the same procedure was employed with synthetic air as the carrier gas.

The oxidation behavior of the pyrolyzed nonwovens was evaluated by static oxidation at 600 °C for 1 h (5 K·min^{-1}) in an industrial furnace.

3. Results and discussion

3.1. Characterization of polymer solutions and electrospun fibers

The electrospinnability of a polymer solution is strongly affected by its rheological properties. Thus, the rheology of the solutions with different silazane systems was first investigated. In general, the solution should be a non-Newtonian shear-thinning fluid, displaying both plastic and elastic properties to support stretching, acceleration and whipping during electrospinning. Pseudoplastic behavior was observed in all solution systems (Fig. 1a). As expected, the solutions containing the polysilazane HTTS resulted in higher viscosities compared to the solutions containing the oligosilazane D1800 due to the higher molecular weight derived from the previous selective polymerization step [29]. Despite the higher molecular weight of PAN, the HTTS_PAN solution was the most viscous. In contrast, the viscosity of PAN_D1800 is higher than D1800_PAN at a low shear rate, suggesting that the oligomeric silazane has a small contribution to the solution viscosity. The D1800_PAN solution has a higher concentration of low molecular weight silazane molecules, and consequently, its contribution to the pseudoplastic behavior is irrelevant.

The electric conductivity indicates the number of electric charges found on the surface of the polymer solution to be electrospun and controls its tendency to form fibers during electrospinning. The solutions PAN_D1800 and PAN_HTTS showed a greater ability to conduct electric current resulting from the higher amount of solvent (Fig. 1b). When dissolving a polymer in a solvent, the conductivity of the solution increases due to the availability of ionic species in the polymer. However, with increasing concentration of the polymer in the solution, the electrical conductivity may decrease. The HTTS_PAN and D1800_PAN solutions showed a conductivity of respectively 14 and 16 µS·cm^{-1}. In contrast, the conductivity of PAN_HTTS and PAN_D1800 solutions was 44 and 54 µS·cm^{-1} caused by the lower polymer concentration.

Beyond viscoelastic properties, the surface tension of polymer

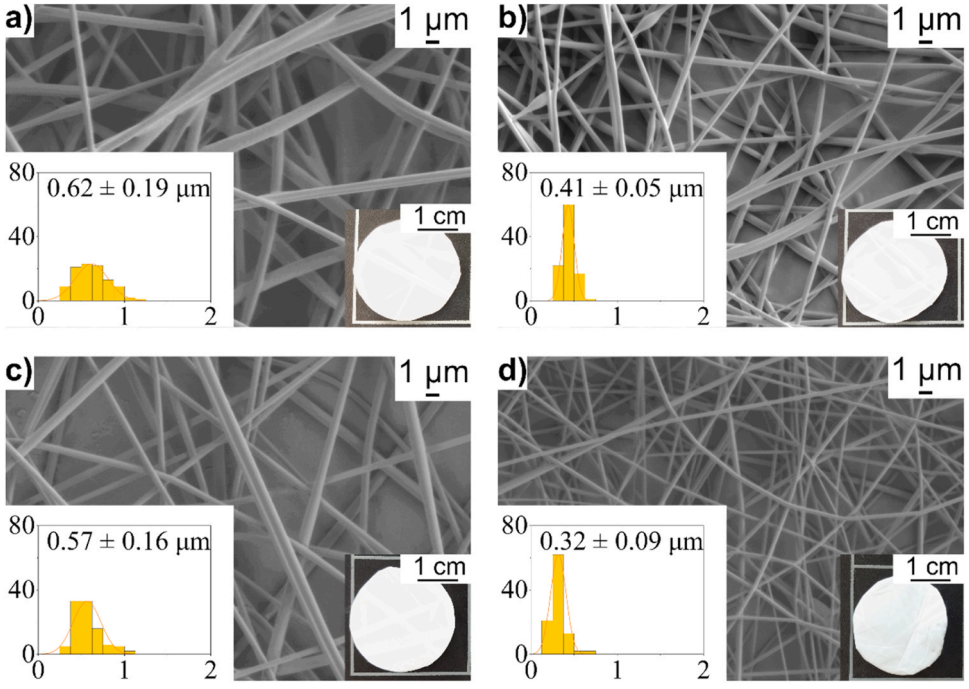

Fig. 2. SEM images showing mean fiber diameter of the nonwovens, respective histogram, and sample photo of a) D1800_PAN, b) HTTS_PAN, c) PAN_D1800, and d) PAN_HTTS.

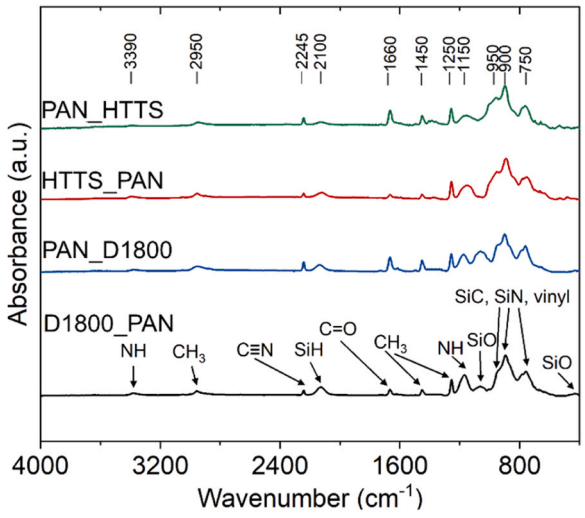

Fig. 3. FTIR-ATR spectra of the as-spun samples.

solution is among the key parameters of the electrospinning process [27]. A polymer solution is elongated when the electrical force overcomes the surface tension, forming consequently fibers in the electrospinning process. The presence of silazane decreased the surface tension of the solution when compared to pure DMF (35 mN·m^{-1} at 20 °C) [30]. D1800 has a shorter backbone chain and a higher percentage of polar groups (N-H and Si-H) than HTTS. The D1800 molecules were thus strongly bonded to one another, which gave the D1800_PAN and PAN_D1800 polymer solutions a high surface tension. Nevertheless, the solutions showed no noteworthy difference in surface tension and these values are very similar to pure solutions of silazane and PAN [27].

After electrospinning, very thin fibers ranging from 0.32 μm to 0.62 μm were obtained (Fig. 2). This indicated that the solutions have the proper viscoelastic, conductivity and surface tension properties to form fibers under the chosen processing parameters. To understand how the solution properties influenced the fiber size and distribution, the explanation needs to be divided into two systems: (1) with more PAN and (2) with more silazane. When there was more PAN, the organic polymer ended up governing the rheology behavior of the system, and the predicted reduction in fiber diameter was noticed for the low-viscosity PAN/D1800 solution. In contrast, for the system with more silazane, the sample D1800/PAN showed a larger average fiber diameter, even though it has a significantly lower viscosity. As in this case the difference in molecular weight was higher (the oligosilazane is liquid at room temperature), this could lead to phase separation of the lower molecular weight oligomers presenting in D1800, causing instability during electrospinning. However, in both samples containing the solid polysilazane HTTS, more uniform fibers (lower dispersion) were obtained when compared with the solutions containing oligosilazane, demonstrating the positive contribution of increasing the silazane molecular weight for electrospinning.

To further understand the influence of silazane on the fiber nonwoven composition, FTIR analyses were conducted. The expected absorption bands were in general agreement with the literature [26,29,31,32] and all materials possess the characteristic peaks of PAN and silazanes (Fig. 3). The presence of silazane was confirmed by the bands at ~3390 and ~1150 cm^{-1} from N-H stretching [ν_s(NH)] and N-H bending [δ_s(NH)]. The symmetric C-H stretching at ~2950 cm^{-1} [ν_s(CH$_3$)] and the symmetric C-H deformation band at ~1450 and 1250 cm^{-1} [δ_s(CH$_3$)] were also identified. The band at ~2100 cm^{-1} was assigned to the symmetric Si-H stretching [ν_s(SiH)]. The vinyl group, Si-C, and Si-N bending bands were determined between 750–950 cm^{-1}. PAN, on the other hand, can be identified by the presence of the C≡N stretching band at ~2245 cm^{-1}.

The most significant differences between the spectra were observed when analyzing the samples in the systems with more PAN and in the systems with more D1800. The samples with more PAN seemed to have more residual DMF (more intense carbonyl peak) due to the high affinity of the polar groups of PAN and DMF as reported elsewhere [33]. On the other hand, the D1800-derived samples had a more intense Si-O peak. HTTS is less susceptible to reactions with moisture than D1800 because it has already been crosslinked reducing the reactive Si-H and N-H groups. As the process was conducted in a nitrogen atmosphere, the

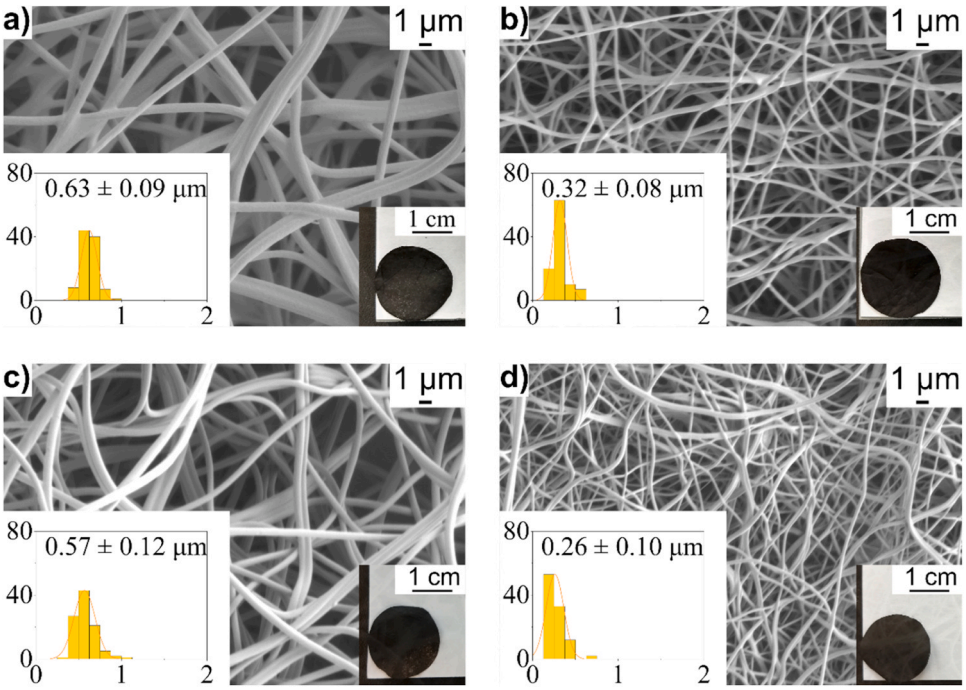

Fig. 4. SEM images showing mean fiber diameter, respective histogram, and optical images of a) D1800_PAN_1000, b) HTTS_PAN_1000, c) PAN_D1800_1000, and d) PAN_HTTS_1000.

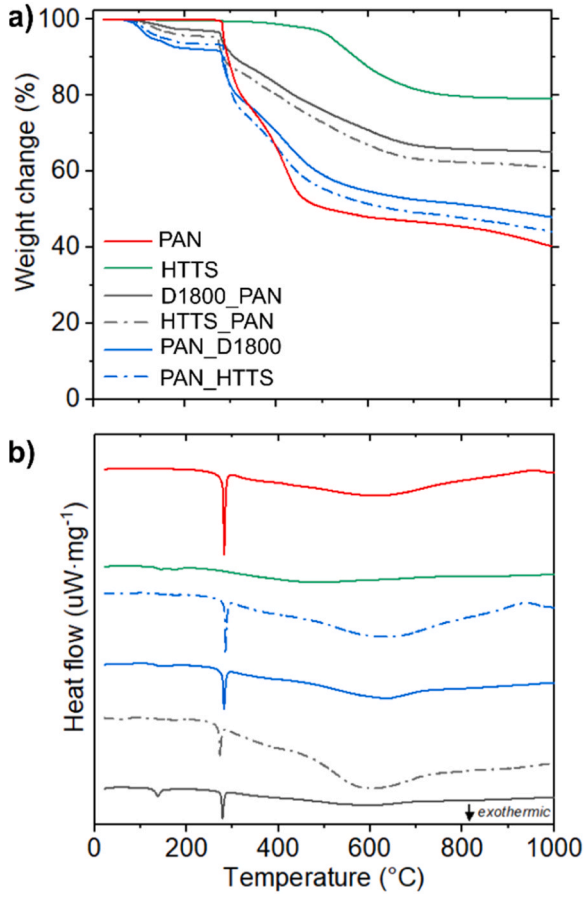

Fig. 5. Curves of a) TGA and b) DSC measurements of as-spun nonwovens pyrolyzed in nitrogen atmosphere.

oxygen contamination was likely to be caused by the DMF solvent, which is highly hydrophilic and can contain residual water impurities [33]. Therefore, FTIR-ATR analysis suggests that the samples prepared with D1800 contained more oxygen in the composition, also confirmed by XPS analysis.

3.2. Investigation of the pyrolysis behavior

During pyrolysis up to 1000 °C in nitrogen, the shrinkage in diameter of the HTTS_PAN_1000C fibers was 22% and 19% for PAN_HTTS_1000 (Fig. 4). Similar results were reported for pure HTTS fibers pyrolyzed at the same conditions [34]. Surprisingly, the ceramic fibers derived from the systems containing the oligomer D1800 seem to have a negligible change in their average diameter, which would indicate zero shrinkage. However, this unusual observation may be explained by fiber coalescence during pyrolysis. Although the radical initiator DCP (3 wt% DCP in relation to the silazane) was employed as a curing agent to prevent coalescence, the concentration was too low to complete the crosslinking of the D1800 before the ceramic transformation because diluting effect of PAN. This coalescence phenomenon was also observed in the HTTS system but to a much lower extent due to previous selective polymerization of the silazane.

To better understand the organic-inorganic transformation during pyrolysis, TGA and DSC measurements were performed. The measured ceramic yields were 65% (D1800_PAN_1000), 61% (HTTS_PAN_1000), 48% (PAN_D1800_1000), and 44% (PAN_HTTS_1000) which are all between pure HTTS (80%) and PAN (40%) (Fig. 5a). According to TGA analysis, all samples showed a first weight loss at 150 °C associated with residual DMF vaporization. As confirmed by FTIR, samples with more PAN present more DMF after electrospinning resulting in higher weight losses up to 150 °C.

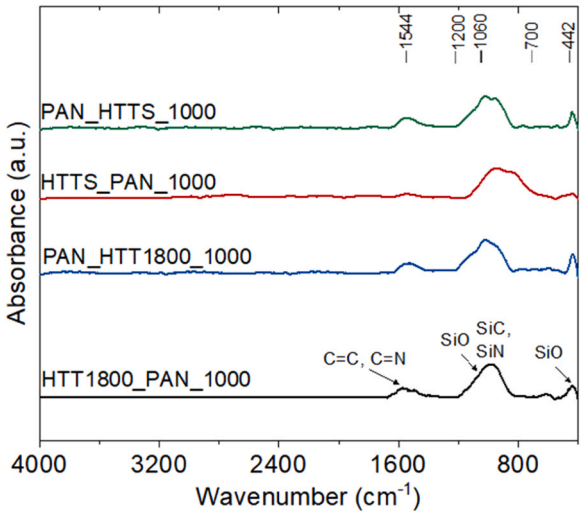

Fig. 6. FTIR-ATR spectra of pyrolyzed samples.

The largest weight change occurred between ~200–400 °C associated with the loss of oligomers for silazane and the release of hydrogen and small quantities of ammonia for both silazane precursors [33]. Normally the sample containing D1800 would have a higher weight loss compared to HTTS in the temperature range of 200–400 °C since D1800 has a higher amount of more volatile oligomers. The fact that this was not observed in the present study suggests some hypothesis. The most likely possibility would be the partial elimination of lower molecular weight oligomers already during electrospinning due to the high voltage applied. Another option could be related to additional crosslinking reactions between the remaining silazane molecules [35] or because of reactions between the Si-H groups from the silazane with N-functionalities from PAN [33]. Finally, more Si-O-Si bonds were detected in the FTIR spectra, which is an indication of an additional crosslinking and the incorporation of oxygen leading to lower weight loss.

Between 400–1000 °C, the main products released from PAN are hydrogen, cyanide, ammonia, and nitrogen [36] and from silazane are hydrocarbons such as methane and hydrogen.

The precursors have two main exothermic peaks at 250–300 °C and 500–700 °C, which correspond to the cyclization and decomposition of PAN (Fig. 5b). The smaller peak at ~600 °C for D1800_PAN suggests the reaction between functional groups of these two precursors. The small exothermic peak at ~125 °C can be attributed to the polymerization initiated by DCP, mainly for the D1800_PAN sample containing Si-H and vinyl groups via vinyl polymerization and hydrosilylation reactions.

3.3. Characterization of the C-rich ceramic phase formation

The conversion of the polymers to ceramics at 1000 °C was confirmed by the disappearance of the N-H and Si-H absorption bands as well as methyl and vinyl groups in the FTIR-ATR of the pyrolyzed samples (Fig. 6). Likewise, the conversion of PAN to ladder structure carbon was observed by the disappearance of the C≡N absorption band. The wide peak between 700 and 1200 cm^{-1} in the pyrolyzed samples is attributed to the formation of SiCN derived from the silazanes [δ_s(SiC) and δ_s(SiN)], while the band at ~1544 cm^{-1} is attributed to C=C and C=N bands [ν_s(C=C) and ν_s(C=N)]. Characteristic peaks at ~442 cm^{-1} and ~1060 cm^{-1} for Si-O stretching [δ_s(Si-O)] were observed mainly for D1800-derived samples, which is ascribed to oxygen incorporation during the experiments [33,37,38].

The formed carbon structure was further evaluated by XRD and Raman analyses. Broad diffraction bands displayed in the XRD patterns were indexed to free carbon ascribed to the (0 1 0) plane of graphite

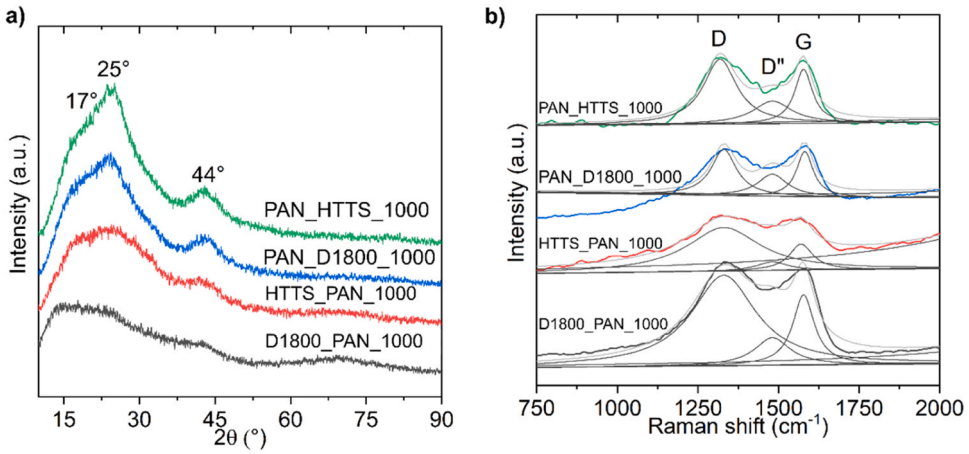

Fig. 7. a) XRD patterns and b) Raman spectra of the C-rich SiCN(O) nonwovens.

Table 2
Raman spectroscopy features of C-rich SiCN(O) nonwovens.

Sample	I_D/I_G	L_a (nm)	$I_D/I_{D''}$	*D* intensity (a.u.)	*D''* intensity (a.u.)	*G* intensity (a.u.)
D1800_PAN_1000	1.29	3.85	3.26	1330	1481	1578
HTTS_PAN_1000	1.67	2.97	4.91	1330	1481	1570
PAN_D1800_1000	1.02	4.84	2.09	1330	1481	1582
PAN_HTTS_1000	1.20	4.14	2.86	1319	1481	1578

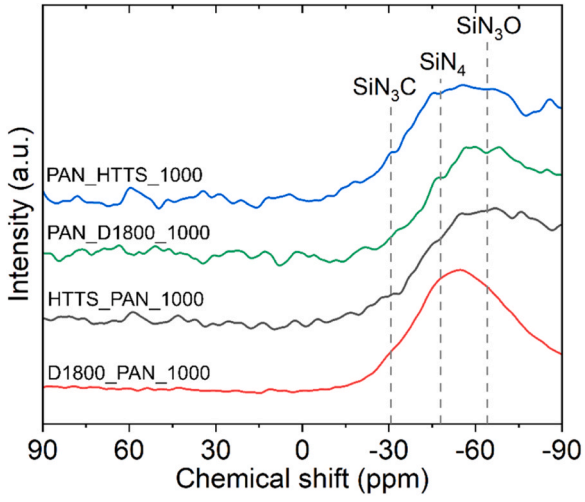

Fig. 8. Solid-state ^{29}Si-NMR of samples heat-treated at 1000 °C in nitrogen atmosphere.

(band at 17°), the (0 0 2) lattice of typical graphite (band at 25°) and the (1 0 0) plane from arbitrary diffraction related to graphene sheets (band at 44°) [39–41] (Fig. 7a). According to XRD patterns, the C-rich SiCN(O) samples were composed of an amorphous structure since diffraction bands showed a diffuse scattering state. Although transmission electron microscopy (TEM) was not carried out in this study, the formation of nanocrystalline structures cannot be ruled out, as these structures would not be detected by XRD [17,42].

Following XRD results, Raman spectroscopy also indicated the existence of a free amorphous carbon phase (Fig. 7b). The characteristic carbon vibrations appeared in all spectra: the *D* band at ~1326 cm^{-1}, the *D''* band at ~1458 cm^{-1} and the *G* band at ~1575 cm^{-1}. The *D* band results from disorder and defect-induced vibration modes of graphene layers in the carbon phase, linked to the breathing motion of sp^2-rings, the *D''* peak arises from amorphous carbon and the *G* mode from an in-plane bond stretching of sp^2-hybridized carbon atoms [43,44]. For samples containing a higher content of silazane, the *D-band* is the strongest band revealing the presence of a disordered graphite. The results indicated that both defective amorphous carbon and ordered crystalline carbon exist in the C-rich SiCN(O).

To better compare the carbon phase ordering, the ratios between the peak intensities are presented in Table 2. The I_D/I_G ratios of the systems containing more silazane are higher, as well as the $I_D/I_{D''}$. These two relationships reveal a more organized carbon phase, especially in the system containing HTTS. This higher ordering level must be related to the contribution of free carbon derived from silazane. Due to the different mechanisms of free carbon formation, there is a greater tendency towards ordering in PDCs, probably due to the more localized generation of free carbon. By contrast, a more considerable portion of sp^3 carbon was expected in PAN-derived samples at this pyrolysis temperature [45].

To evaluate the molecular structure of the obtained C-rich SiCN(O), ^{29}Si-NMR spectroscopy was conducted (Fig. 8). Broad resonances dominated at −48 ppm assigned to silicon bonds in SiN_4 [33]. The formation of SiN_3C is more intense in D1800_PAN_1000. The possibility of the existence of a small amount of other mixed bonds, such as SiC_4 and SiC_2N_2, cannot be excluded. As mentioned before, during pyrolysis additional Si-N bonds between the silazane and PAN can be formed, which favors the formation of SiN_4 sites [33,46]. The ^{29}Si-NMR spectra showed a −65 ppm peak assigned to SiN_3O environments [47], limiting more conclusions from this technique due to the high amount of oxygen. The chemical shift corresponding to SiO_4 is usually detected at −110.8 ppm [47,48]. Here SiO_4 was not detected in the NMR spectra due to limitations in the equipment, however, the presence of SiO_4 in the materials cannot be ruled out.

XPS spectroscopy can measure the elemental composition as well as the chemical and electronic state of the atoms but only on the surface of the fibers. However, considering the care taken in handling and preparation of the sample, as described in the experimental procedure, and the fact that the fiber diameters are in the submicrometer scale, the XPS results can indicate the composition of the sample as a whole. According to the molecular composition determined by XPS, all manufactured

Table 3
Elemental compositions of the surface of C-rich SiCN(O) nonwovens determined with XPS analyses.

Sample	*Composition (at%)*				Free carbon (mol.%)
	Si	*C*	*N*	*O*	
D1800_PAN_1000	19.6	52.1	5.4	22.9	59.7
HTTS_PAN_1000	28.6	39.7	18.5	13.2	43.6
PAN_D1800_1000	15.2	55.2	4.9	24.7	64.4
PAN_HTTS_1000	16.3	54.3	9.5	19.9	62.9

electrospun nonwovens are definitively C-rich PDCs (Table 3). A higher oxygen presence occurred with samples derived from D1800 due to the greater amount of active sites to react with oxygen, confirming the results detected by FTIR-ATR and ^{29}Si-NMR measurements. XPS analysis suggested that a higher content of Si was obtained in samples with the polysilazane HTTS. High-resolution XPS spectra under the Si 2p band indicated the presence of Si-N (101.9 eV), Si-C (102.7 eV), and Si-O (103.5 eV) peaks [49,50]; under C 1 s band with C-Si (284.0 eV), C-C (284.9 eV), and C═O (286.0 eV) peaks; under N 1 s band with N-Si (397.3 eV) and N-C (400.4 eV) peaks [51,52]; and O 1 s band with O-Si (532.4 eV) and C═O (534.0 eV) peaks [53] (Fig. 9). The Si 2p XPS spectra are in good agreement with the ^{29}Si-NMR results, in which different silicon environments were observed. The N 1 s XPS spectrum suggests a higher concentration of N-Si chemical bonds in HTTS_PAN_1000 fiber surface than in D1800_PAN_1000 fiber surface. The increased amount of carbon in the fiber nonwoven derived from D1800 led to a higher intensity of the C-C peak. Furthermore, the samples with more PAN seemed to be very similar in terms of the amount of carbon and silicon, resulting in a comparable quantity of free carbon. However, there was a big difference between the HTTS- and D1800-derived samples. As previously discussed the D1800 oligosilazane may volatilize partially during electrospinning because of very low

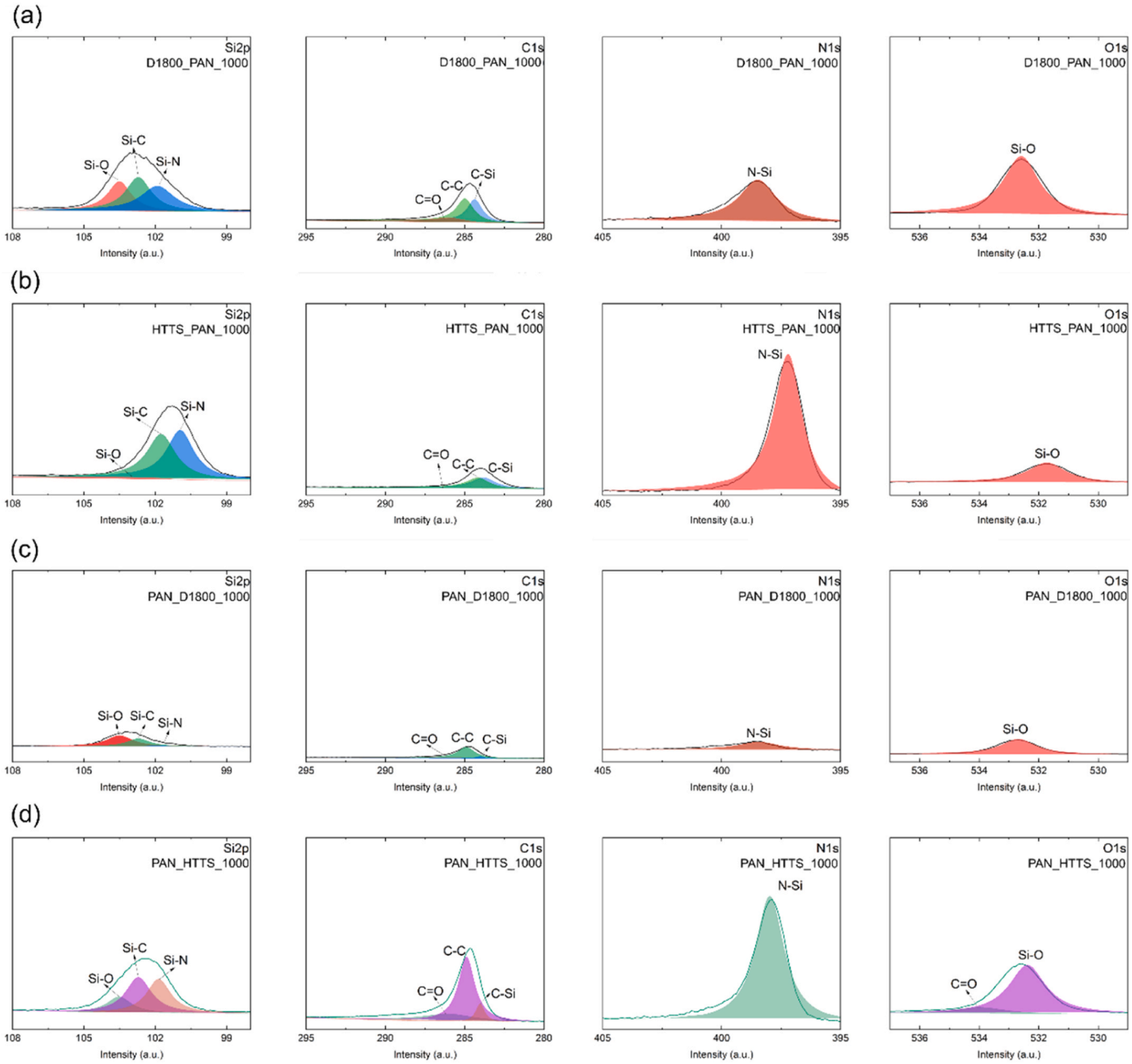

Fig. 9. High-resolution XPS spectra of the (a) D1800_PAN_1000, (b) HTTS_PAN_1000, (c) PAN_D1800_1000 and (d) PAN_HTTS_1000 nonwovens.

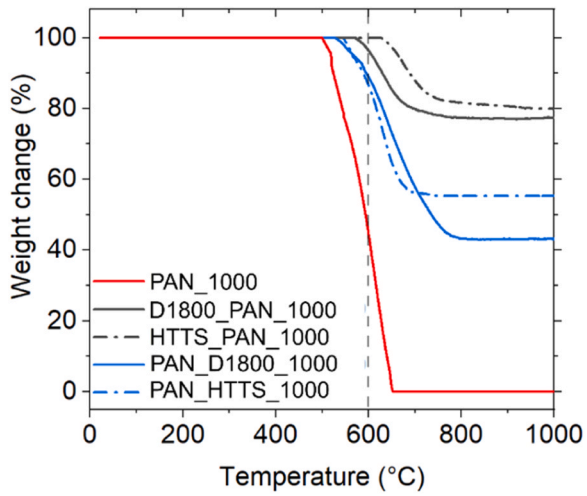

Fig. 10. Curves of TGA of C-rich SiCN(O) and carbon nonwovens for oxidation resistance evaluation (heating rate: 5 K·min^{-1}; atmosphere: synthetic air).

molar weight molecules and is therefore not fully incorporated into the fiber.

3.4. Oxidation resistance

TGA measurements were performed in flowing synthetic air to assess the oxidation resistance of the nonwovens (Fig. 10). For comparison, a carbon fiber nonwoven was manufactured from PAN (PAN_1000) under similar conditions and tested accordingly.

For all samples, an increase in thermo-oxidative resistance was observed by the shifting of the onset oxidation temperature: HTTS_PAN_1000 (ca. 627 °C), PAN_HTTS_1000 (ca. 546 °C), D1800_PAN_1000 (ca. 572 °C), PAN_D1800_1000 (ca. 528 °C). In comparison, the onset oxidation temperature for PAN_1000 is at about 500 °C. The oxidation resistance of the material in this study is determined by how well the ceramic phase can protect the carbon from oxidizing, being proportional to the amount and distribution of the carbon phase in the matrix. For this reason, samples with more carbon performed worse in the oxidation test.

Remarkably at 1000 °C, the samples derived from polysilazane and PAN possess a lower weight loss: 20% for HTTS_PAN_1000, 23% for D1800_PAN_1000, 45% for PAN_HTTS_1000, and 57% for PAN_D1800_1000. The systems with more PAN had little effect on the matrix protection because of the huge amount of free carbon. The advantage of the system with HTTS can be justified by the higher amount of the oxidation-resistant SiCN phase. For the samples with more silazane, the amount of free carbon is lower, leading to a more oxidation-resistant material. The oxidation resistance of the HTTS_PAN_1000 nonwoven is therefore mainly attributed to the chemical composition, molecular structure, and homogeneously distributed free carbon phase within the SiCN(O) matrix. In addition, according to the Raman results of the present study, the HTTS_PAN_1000 sample has more organized carbon, which also contributes to improved oxidation resistance.

In the case of pure SiCN(O) ceramics, usually, the most present free turbostratic carbon is well protected from oxidation by the ceramic phase. After the formation of a dense silica layer at the surface further oxidation is diffusion controlled. However, if the carbon content is too high and/or not well distributed the ceramic phase cannot form a continuous and dense protective layer during oxidation, which leads to a catastrophic loss of oxidation resistance. Thus, ceramics with a high content of free carbon tend to oxidize much faster. Therefore, the high free carbon content in PAN_D1800_1000 and PAN_HTTS_1000 reduced the oxidative resistance due to the exposition of free carbon directly to oxidation, which is the main drawback in high-temperature applications of carbonaceous materials. Ribeiro et al. reported very similar C-rich SiCN materials but synthesized from in situ radical polymerization of acrylonitrile with Durazane 1800 having a similar free-carbon amount to the materials synthesized in the present study. However, the onset oxidation temperature was much higher at about 800 °C (with 60 wt% of silazane) and 650 °C (with only 30 wt% of silazane) [33]. The better phase distribution resulting from the in situ reaction could be responsible for the higher oxidation resistance. Furthermore, it should be noted that the fiber diameter was about 200 µm in contrast to the submicrometer size of the fibers used in this study, which results in a much

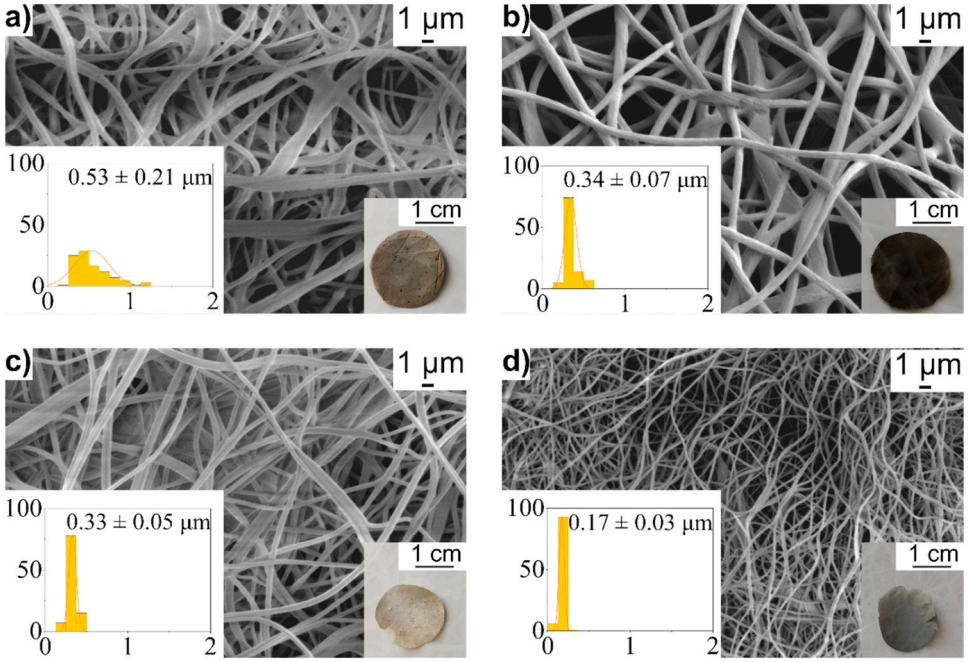

Fig. 11. SEM images containing the respective histogram, mean fiber diameter, and sample photo after oxidation tests at 600 °C for 1 h of a) D1800_PAN_1000, b) HTTS_PAN_1000, c) PAN_D1800_1000, and d) PAN_HTTS_1000.

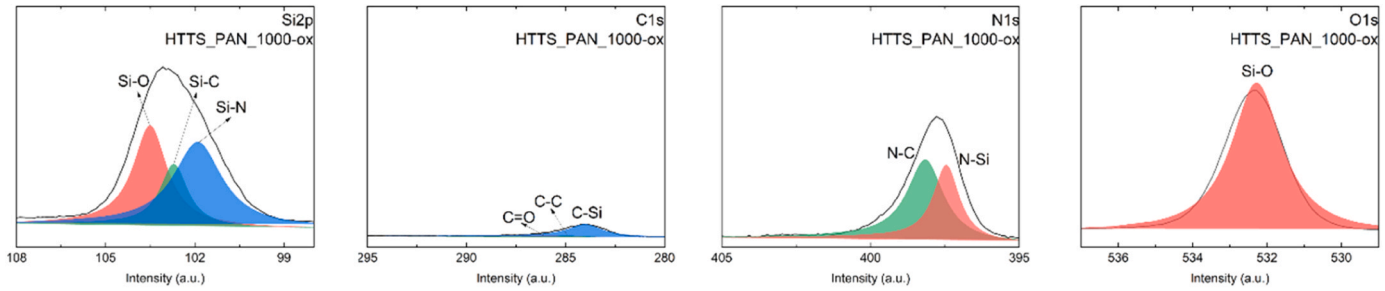

Fig. 12. High-resolution XPS spectra of oxidized HTTS_PAN_1000 nonwoven.

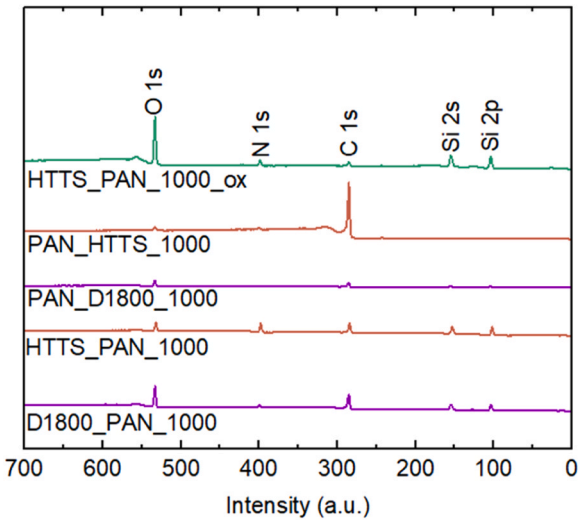

Fig. 13. Survey XPS spectra of oxidized HTTS_PAN_1000 nonwoven in comparison to pristine materials.

higher surface area available for oxidation.

SEM analyses of the nonwovens after the oxidation tests up to 600 °C provide the impression that the fibers remained almost unchanged because no signs of pores or cracks due to oxidation appeared (Fig. 11). However, fiber size reduction, change in sample color, weight loss, and a pronounced brittleness were noticed for D1800_PAN_1000, PAN_D1800_1000, and PAN_HTTS_1000 samples. In contrast, the HTTS_PAN_1000 sample was still almost intact with only a very small decrease in the fiber diameter. XPS analyses of this fiber type revealed an increase in the oxygen content at the surface after oxidation due to the formation of silica and oxygen-containing ceramic phases (Fig. 12). The survey spectra to each sample also showed the increase in the oxygen of oxidized HTTS_PAN_1000 in comparison to the other materials (Fig. 13). Since nitrogen and carbon are still detectable, it is likely that a closed oxidation protection layer composed of silica, SiOCN but also Si_2N_2O was able to form on the surface of HTTS_PAN_1000 sample to protect the segregated carbon [33,54].

The surface area of the nonwovens prepared in this study varied between 2.7 and 6.1 $m^2 \cdot g^{-1}$ with 4.9 $m^2 \cdot g^{-1}$ for the HTTS_PAN_1000 material. Although ceramics based on silazanes already have a low density the electrospun PDCs from the present work showed even lower values of only ~1.8 up to 2.1 $g \cdot cm^{-3}$ which is in the case of the HTTS_PAN_1000 material a reduction of 18% in comparison to bulk SiCN pyrolyzed at 1000 °C [55] and 6.6% to SiCN used as matrix material [56]. This lower density results primarily from the high carbon content.

4. Conclusions

In this study, C-rich SiCN(O) nonwovens were developed via electrospinning of solutions of PAN in combination with several ratios of an oligosilazane (Durazane 1800) or a polysilazane (HTTS synthesized from Durazane 1800) and subsequent pyrolysis. By adjusting the viscosity of the solutions very thin fibers with diameters ranging from 0.32 μm to 0.62 μm were obtained. The subsequent pyrolysis up to 1000 °C in a nitrogen atmosphere led to amorphous C-rich ceramic nonwovens with several Si-C-N-O phases highly dispersed within the fibers. The oxygen contamination was introduced during the handling of the samples, especially by using the more reactive Durazane 1800. Surprisingly, the fiber diameter after pyrolysis at 1000 °C was also determined between 0.26 and 0.63 μm most probably because of fiber coalescence during pyrolysis. The higher oxygen contamination by using the oligosilazane in combination with PAN also led to a higher ceramic yield due to additional crosslinking reactions. A higher initial oxidation temperature compared to pure carbon (~500 °C) was confirmed for all samples. As expected the materials with more PAN had little effect on the matrix protection because the small amount of the formed ceramic phases cannot form a dense passivating layer to protect the high amount of free-carbon. Therefore, the best oxidation resistance up to 600 °C was achieved with sample HTTS_PAN_1000 which contains a higher amount of polysilazane able to form a dense passivating layer for the protection of the free carbon regions. The oxidation resistance of the HTTS_PAN_1000 nonwoven is therefore mainly attributed to the chemical composition and molecular structure of the polymers resulting in a homogeneously distributed free carbon phase within the fiber matrix.

The results suggested that C-rich SiCN(O) nonwovens have a high potential for applications as catalyst support at high temperatures in harsh environments but also as a lightweight material because of their low density.

This work also demonstrated the advantages of the PDC technology that with simple modifications to the composition or chemical structure of the polymers, the properties of the resulting ceramics can be specifically adjusted.

CRediT authorship contribution statement

Heloisa Ramlow: Data curation, Formal analysis, Investigation, Methodology, Validation, Visualization, Writing – original draft. **Luiz Fernando Belchior Ribeiro:** Data curation, Formal analysis, Investigation, Methodology, Validation, Visualization, Writing – original draft. **Stefan Schafföner:** Formal analysis, Validation, Visualization, Writing – review & editing. **Günter Motz:** Conceptualization, Formal analysis, Funding acquisition, Methodology, Project administration, Supervision, Validation, Writing – review & editing. **Ricardo Antonio Francisco Machado:** Conceptualization, Funding acquisition, Project administration, Resources, Supervision.

Declaration of Competing Interest

The authors declare that they have no known competing financial interests or personal relationships that could have appeared to influence the work reported in this paper.

Acknowledgments

This study was financed in part by the Coordenação de Aperfeiçoamento de Pessoal de Nível Superior - Brasil (CAPES) - Finance Code 001. The authors thank CAPES within the project PROBRAL (nº 88887.368756/2019-00), Deutscher Akademischer Austauschdienst (DAAD) Project-ID 57575843 and Deutsche Forschungsgemeinschaft (DFG) (MO 851/21-1 Project-ID 455984818) for supporting this work.

References

[1] Fitria, A. Kumar, M. Dewa, J. Liu, S. Ha, B. Yang, Development of sulfonated carbon-based solid-acid catalysts derived from biorefinery residues and biomass ash for xylan hydrolysis, Bioresour. Technol. Rep. 24 (2023) 101607, https://doi.org/10.1016/j.biteb.2023.101607.

[2] H. Lee, C. Kwon, S. Vikneshvaran, S. Lee, S.-Y. Lee, Partial oxidation of methane to methyl oxygenates with enhanced selectivity using a single-atom copper catalyst on amorphous carbon support, Appl. Surf. Sci. 639 (2023) 158289, https://doi.org/10.1016/j.apsusc.2023.158289.

[3] Z. Zhao, X. Long, M. Millan, G. Yuan, Z. Cui, Z. Dong, Y. Cong, J. Zhang, X. Li, The influence of carbon supports and their surface modification on aqueous phase highly selective hydrogenation of phenol to cyclohexanol over different Ni/carbon catalysts, Carbon 213 (2023) 118227, https://doi.org/10.1016/j.carbon.2023.118227.

[4] J. Liu, C. Tian, T. Jiang, E.I. Ricohermoso, Z. Yu, E. Ionescu, L. Molina-Luna, J. P. Hofmann, R. Riedel, Polymer-derived SiOC ceramics: a potential catalyst support controlled by the sintering temperature and carbon content, J. Eur. Ceram. Soc. 43 (2023) 3191–3200, https://doi.org/10.1016/j.jeurceramsoc.2023.02.045.

[5] Y. Zhang, Y. Zhao, Q. Chen, Y. Hou, Q. Zhang, L. Cheng, L. Zheng, Flexible SiC-CNTs hybrid fiber mats for tunable and broadband microwave absorption, Ceram. Int. 47 (2021) 8123–8132, https://doi.org/10.1016/j.ceramint.2020.11.167.

[6] R. Riedel, G. Mera, R. Hauser, A. Klonczynski, Silicon-based polymer-derived ceramics: synthesis properties and applications - a review, J. Ceram. Soc. Jpn. 114 (2006) 425–444, https://doi.org/10.2109/jcersj.114.425.

[7] R. Schierholz, D. Kröger, H. Weinrich, M. Gehring, H. Tempel, H. Kungl, J. Mayer, R.-A. Eichel, The carbonization of polyacrylonitrile-derived electrospun carbon nanofibers studied by in situ transmission electron microscopy, RSC Adv. 9 (2019) 6267–6277, https://doi.org/10.1039/C8RA10491C.

[8] M. Ma, H. Wang, X. Li, K. Peng, L. Xiong, X. Du, Free-standing SiOC/nitrogen-doped carbon fibers with highly capacitive Li storage, J. Eur. Ceram. Soc. 40 (2020) 5238–5246, https://doi.org/10.1016/j.jeurceramsoc.2020.06.034.

[9] K. Sokolowski, M. Gubernat, S. Blazewicz, A. Fraczek-Szczypta, Comparative study of interphase evolution in polysiloxane resin-derived matrix containing carbon micro and nanofibers during thermal treatment, J. Eur. Ceram. Soc. 40 (2020) 5205–5216, https://doi.org/10.1016/j.jeurceramsoc.2020.07.009.

[10] Y. Iwamoto, G. Motz, E. Ionescu, S. Bernard, Preceramic polymers as precursors of advanced ceramics: the polymer-derived ceramics (PDCs) route. Reference Module in Materials Science and Materials Engineering, Elsevier, 2021, https://doi.org/10.1016/B978-0-12-803581-8.12080-6.

[11] A. Lale, M. Schmidt, M.D. Mallmann, A.V.A. Bezerra, E.D. Acosta, R.A.F. Machado, U.B. Demirci, S. Bernard, Polymer-derived ceramics with engineered mesoporosity: from design to application in catalysis, Surf. Coat. Technol. 350 (2018) 569–586, https://doi.org/10.1016/j.surfcoat.2018.07.061.

[12] A. Viard, P. Miele, S. Bernard, Polymer-derived ceramics route toward SiCN and SiBCN fibers: from chemistry of polycarbosilazanes to the design and characterization of ceramic fibers, J. Ceram. Soc. Jpn. 124 (2016) 967–980, https://doi.org/10.2109/jcersj2.16124.

[13] Q. Tian, N. Wu, B. Wang, Y. Wang, Fabrication of hollow SiC ultrafine fibers by single-nozzle electrospinning for high-temperature thermal insulation application, Mater. Lett. 239 (2019) 109–112, https://doi.org/10.1016/j.matlet.2018.12.077.

[14] P. Colombo, G. Mera, R. Riedel, G.D. Sorarù, Polymer-derived ceramics: 40 years of research and innovation in advanced ceramics, J. Am. Ceram. Soc. 93 (2010) 1805–1837, https://doi.org/10.1002/9783527631971.ch07.

[15] Z. Ren, S. Bin Mujib, G. Singh, High-temperature properties and applications of Si-based polymer-derived ceramics: a review, Materials 14 (2021) 614, https://doi.org/10.3390/ma14030614.

[16] N. Thor, J. Bernauer, N.-C. Petry, E. Ionescu, R. Riedel, A. Pundt, H.-J. Kleebe, Microstructural evolution of Si(Hf_xTa_{1-x})(C)N polymer-derived ceramics upon high-temperature anneal, J. Eur. Ceram. Soc. 43 (2023) 1417–1431, https://doi.org/10.1016/j.jeurceramsoc.2022.11.060.

[17] L. Ribeiro, A. Bezerra, C. Gervais, S. Bernard, R. Machado, G. Motz, The influence of pyrolysis temperature on the oxidation resistance of carbon-rich SiCN ceramics derived from reaction of silazanes with acrylonitrile, J. Eur. Ceram. Soc. 41 (2021) 3285–3291, https://doi.org/10.1016/j.jeurceramsoc.2021.01.042.

[18] L.M. Reinold, M. Graczyk-Zajac, Y. Gao, G. Mera, R. Riedel, Carbon-rich SiCN ceramics as high capacity/high stability anode material for lithium-ion batteries, J. Power Sources 236 (2013) 224–229, https://doi.org/10.1016/j.jpowsour.2013.02.046.

[19] M. Graczyk-Zajac, L.M. Reinold, J. Kaspar, P.V.W. Sasikumar, G.D. Soraru, R. Riedel, New insights into understanding irreversible and reversible lithium storage within SiOC and SiCN ceramics, Nanomaterials 5 (2015) 233–245, https://doi.org/10.3390/nano5010233.

[20] L.M. Reinold, Y. Yamada, M. Graczyk-Zajac, H. Munakata, K. Kanamura, R. Riedel, The influence of the pyrolysis temperature on the electrochemical behavior of carbon-rich SiCN polymer-derived ceramics as anode materials in lithium-ion batteries, J. Power Sources 282 (2015) 409–415, https://doi.org/10.1016/j.jpowsour.2015.02.074.

[21] M. Storch, D. Vrankovic, M. Graczyk-Zajac, R. Riedel, The influence of pyrolysis temperature on the electrochemical behavior of porous carbon-rich SiCN polymer-derived ceramics, Solid State Ion. 315 (2018) 59–64, https://doi.org/10.1016/j.ssi.2017.11.032.

[22] C. Bäumler, C. Bauer, R. Kempe, The synthesis of primary amines through reductive amination employing an iron catalyst, ChemSusChem 13 (2020) 3110–3114, https://doi.org/10.1002/cssc.202000856.

[23] T. Schönauer, S.L.J. Thomä, L. Kaiser, M. Zobel, R. Kempe, General synthesis of secondary alkylamines by reductive alkylation of nitriles by aldehydes and ketones, Chem. Eur. J. 27 (2021) 1609–1614, https://doi.org/10.1002/chem.202004755.

[24] K. Ge, L. Ye, W. Han, Y. Han, C. Xu, T. Zhao, Si(B)CN-doped carbon nanofibers with excellent oxidation resistance, Mater. Lett. 112 (2013) 124–128, https://doi.org/10.1016/j.matlet.2013.08.122.

[25] X. Liao, J. Denk, T. Tran, N. Miyajima, L. Benker, S. Rosenfeldt, S. Schafföner, M. Retsch, A. Greiner, G. Motz, S. Agarwal, Extremely low thermal conductivity and high electrical conductivity of sustainable carbon-ceramic electrospun nonwoven materials, Sci. Adv. 9 (2023), https://doi.org/10.1126/sciadv.ade6066.

[26] O. Flores, T. Schmalz, W. Krenkel, L. Heymann, G. Motz, Selective cross-linking of oligosilazanes to tailored meltable polysilazanes for the processing of ceramic SiCN fibres, J. Mater. Chem. A 1 (2013) 15406–15415, https://doi.org/10.1039/c3ta13254d.

[27] H. Ramlow, C. Marangoni, G. Motz, R.A.F. Machado, Statistical optimization of polysilazane-derived ceramic: electrospinning with and without organic polymer as a spinning aid for manufacturing thinner fibers, Chem. Eng. J. Adv. 9 (2022) 100220, https://doi.org/10.1016/j.ceja.2021.100220.

[28] Q. Wen, Z. Yu, R. Riedel, The fate and role of in situ formed carbon in polymer-derived ceramics, Prog. Mater. Sci. 109 (2020) 100623, https://doi.org/10.1016/j.pmatsci.2019.100623.

[29] R. Chavez, E. Ionescu, C. Balan, C. Fasel, R. Riedel, Effect of ambient atmosphere on crosslinking of polysilazanes, J. Appl. Polym. Sci. 119 (2011) 794–802, https://doi.org/10.1002/app.

[30] I.M. Smallwood, Handbook of Organic Solvent Properties, Arnold, London, 1996, https://doi.org/10.1016/C2009-0-23646-4.

[31] Y. Feng, S. Dou, Y. Wei, Y. Zhang, X. Song, X. Li, V.S. Battaglia, Preparation and capacity-fading investigation of polymer-derived silicon carbonitride anode for lithium-ion battery, ACS Omega 2 (2017) 8075–8085, https://doi.org/10.1021/acsomega.7b01462.

[32] L. Zhang, Z. Liu, Y. Dai, R. Jin, TG-FTIR study of degradation mechanism and pyrolysis products of high molecular polyacrylonitrile with different oxidation degree, Asian J. Chem. 25 (2013) 8797–8802, https://doi.org/10.14233/ajchem.2013.15711.

[33] L.F.B. Ribeiro, O. Flores, P. Furtat, C. Gervais, R. Kempe, R.A.F. Machado, G. Motz, A novel PAN/silazane hybrid polymer for processing of carbon-based fibres with extraordinary oxidation resistance, J. Mater. Chem. A 5 (2017) 720–729, https://doi.org/10.1039/c6ta09293d.

[34] L.F.B. Ribeiro, R.S. Cunha, A. de Noni, R.A.F. Machado, G. Motz, S.Y.G. González, Flexible and porous nonwoven SiCN ceramic material via electrospinning of an optimized silazane solution, Adv. Eng. Mater. 7 (1) (2021) 2100321, https://doi.org/10.1002/adem.202100321.

[35] G. Motz, S. Schmidt, S. Beyer, The PIP-process: precursor properties and applications, in: W. Krenkel (Ed.), Ceramic Matrix Composites: Fiber Reinforced Ceramics and their Applications, 2008, pp. 165–186. ⟨https://doi.org/10.1002/9783527622412.ch7⟩.

[36] S.M. Saufi, A.F. Ismail, Development and characterization of polyacrylonitrile (PAN) based carbon hollow fiber membrane, Songklanakarin J. Sci. Technol. 24 (2002) 843–854. ⟨http://eprints.utm.my/141/⟩.

[37] G. Motz, T. Schmalz, S. Trassl, R. Kempe, Oxidation behavior of SiCN materials, in: S. Bernard (Ed.), Design, Processing & Properties of Ceramic Materials from Preceramic Precursors, Nova Science Publishers Inc., Hauppauge USA, 2011, pp. 15–35.

[38] E. Bernardo, L. Fiocco, G. Parcianello, E. Storti, P. Colombo, Advanced ceramics from preceramic polymers modified at the nano-scale: a review, Materials 7 (2014) 1927–1956, https://doi.org/10.3390/ma7031927.

[39] S.W. Choi, J.R. Kim, S.M. Jo, W.S. Lee, Y.-R. Kim, Electrochemical and spectroscopic properties of electrospun PAN-based fibrous polymer electrolytes, J. Electrochem. Soc. 152 (2005) A989, https://doi.org/10.1149/1.1887166.

[40] S.A. Smith, B.P. Williams, Y.L. Joo, Effect of polymer and ceramic morphology on the material and electrochemical properties of electrospun PAN/polymer derived ceramic composite nano fiber membranes for lithium ion battery separators, J. Membr. Sci. 526 (2017) 315–322, https://doi.org/10.1016/j.memsci.2016.12.052.

[41] Y.S. Kim, Y.L. Joo, Y.J. Kwark, Highly stable silicon-carbon-nitrogen composite anodes from silsesquiazane for rechargeable lithium-ion battery, J. Mater. Sci. Technol. 32 (2016) 195–199, https://doi.org/10.1016/j.jmst.2015.12.019.
[42] G. Mera, R. Riedel, F. Poli, K. Müller, Carbon-rich SiCN ceramics derived from phenyl-containing poly(silylcarbodiimides), J. Eur. Ceram. Soc. 29 (2009) 2873–2883, https://doi.org/10.1016/j.jeurceramsoc.2009.03.026.
[43] M. Graczyk-Zajac, C. Fasel, R. Riedel, Polymer-derived-SiCN ceramic/graphite composite as anode material with enhanced rate capability for lithium ion batteries, J. Power Sources 196 (2011) 6412–6418, https://doi.org/10.1016/j.jpowsour.2011.03.076.
[44] M. Wilamowska, V.S. Pradeep, M. Graczyk-Zajac, R. Riedel, G.D. Sorarù, Tailoring of SiOC composition as a way to better performing anodes for Li-ion batteries, Solid State Ion. 260 (2014) 94–100, https://doi.org/10.1016/j.ssi.2014.03.021.
[45] H. Ramlow, G.B. de Souza, M.P. Fonseca, A. Raizer, C.R. Rambo, R.A.F. Machado, Lightweight and flexible nanostructured C/SiCN nanofiber nonwoven for electromagnetic reflection shielding of 5G C-Band frequencies, J. Mater. Sci. Mater. Electron. 34 (2023) 1631, https://doi.org/10.1007/s10854-023-11037-x.
[46] S. Traßl, D. Suttor, G. Motz, E. Rössler, G. Ziegler, Structural characterisation of silicon carbonitride ceramics derived from polymeric precursors, J. Eur. Ceram. Soc. 20 (2000) 215–225, https://doi.org/10.1016/s0955-2219(99)00142-9.
[47] S. Kohn, W. Hoffbauer, M. Jansen, R. Franke, S. Bender, Evidence for the formation of SiON glasses, J. Non Cryst. Solids 224 (1998) 232–243, https://doi.org/10.1016/S0022-3093(97)00467-5.
[48] J.W. Wang, L. Lin, J.-Q. Gu, M.-Y. Yang, X. Xu, C.-S. Chen, H.-T. Wang, S. Agathopoulos, Highly stable hydrophobic SiNCO nanoparticle-modified silicon nitride membrane for zero-discharge water desalination, AIChE J. 63 (2017) 1272–1277, https://doi.org/10.1002/aic.
[49] L. David, R. Bhandavat, U. Barrera, G. Singh, Silicon oxycarbide glass-graphene composite paper electrode for long-cycle lithium-ion batteries, Nat. Commun. 7 (2016) 10998, https://doi.org/10.1038/ncomms10998.
[50] Y. Feng, N. Feng, Y. Wei, Y. Bai, Preparation and improved electrochemical performance of SiCN-graphene composite derived from poly(silylcarbondiimide) as Li-ion battery anode, J. Mater. Chem. A 2 (2014) 4168–4177, https://doi.org/10.1039/c3ta14441k.
[51] M.A. Abass, A.A. Syed, C. Gervais, G. Singh, Synthesis and electrochemical performance of a polymer-derived silicon oxycarbide/boron nitride nanotube composite, RSC Adv. 7 (2017) 21576–21584, https://doi.org/10.1039/c7ra01545c.
[52] X. Guo, J. Lu, J. Liu, C. Liu, Y. Tong, J. Li, H. Sun, H. Peng, S. Wu, Y. Feng, H. Gong, Enhanced electromagnetic wave absorption properties of PDCs-SiCN(Ni) fibers by in-situ formed CNTs and Ni2Si, Ceram. Int. (2022), https://doi.org/10.1016/j.ceramint.2022.04.012.
[53] S.Bin Mujib, F. Ribot, C. Gervais, G. Singh, Self-supporting carbon-rich SiOC ceramic electrodes for lithium-ion batteries and aqueous supercapacitors, RSC Adv. 11 (2021) 35440–35454, https://doi.org/10.1039/d1ra05968h.
[54] A. Viard, H. Kurz, A. Lale, L. Heymann, B. Weber, S. Bernard, M. Knauer, G. Motz, Superparamagnetic silicon carbonitride ceramic fibers through in situ generation of iron silicide nanoparticles during pyrolysis of an iron-modified polysilazane, Appl. Mater. Interfaces 13 (2021) 8745–8753, https://doi.org/10.1021/acsami.0c20885.
[55] Y. Li, Y. Yua, H. San, Y. Chen, D. Guo, X. Wu, Full dense SiCN ceramics derived from polysilazane, Adv. Mater. Res. 631–632 (2013) 303–305, https://doi.org/10.4028/www.scientific.net/AMR.631-632.303.
[56] B. Mainzer, C. Lin, R. Jemmali, M. Frieß, R. Riedel, D. Koch, Characterization and application of a novel low viscosity polysilazane for the manufacture of C- and SiC-fiber reinforced SiCN ceramic matrix composites by PIP process, J. Eur. Ceram. Soc. 39 (2019) 212–221, https://doi.org/10.1016/j.jeurceramsoc.2018.09.042.